1993

A Semi-Linear Elliptic PDE Model for the Static Solution of Josephson Junctions

J. G. Caputo

N. Flytzanis

E. A. Vavalis

Report Number:
93-049

A Semi-Linear Elliptic PDE Model for the Static Solution of Josephson Junctions

J.G. Caputo[1], N. Flytzanis[2]
and E.A. Vavalis[3]

CSD-TR-93-049
July 1993

A SEMI-LINEAR ELLIPTIC PDE MODEL FOR THE STATIC SOLUTION OF JOSEPHSON JUNCTIONS

J. G. CAPUTO*, N. FLYTZANIS† AND E.A. VAVALIS‡

Abstract. In this study we derive a semi-linear Elliptic Partial Differential Equation (PDE) problem that models the static (zero voltage) behavior of a Josephson window junction. Iterative methods for solving this problem are proposed, analyzed and their convergence analysis is presented. The preliminary computational results that are given, show the modeling power of our approach and exhibit its computational efficiency.

1. Introduction. Josephson junction devices have been extensively used in many applications like very sensitive magneto-meters, high frequency oscillators, fast switches etc. To study and analyze such devices, differential equation problems that model them have been widely used. In this paper we present a semi-linear elliptic PDE problem which effectively and accurately models the static behavior of a 2-dimensional Josephson window junction. The existence of the solutions and the analysis of their smoothness and stability are not addressed here. Efficient and stable numerical methods are proposed to solve this PDE problem and a software infrastructure that can be used as a simulation engine for Josephson junction devices is presented.

The rest of the paper is organized as follows. In Section 2 we present the derivation of the PDE problem that models the Josephson junction. A brief discussion about the underlying physics and a list of applications based on the Josephson junction are also given. In Section 3 numerical algorithms for solving the derived PDE problem are presented, their convergence analysis is discussed and certain implementation issues are addressed. In Section 4, preliminary numerical experiments that confirm the convergence properties of the method, as well its efficiency, are presented. A list of plots concerning the characteristics of the computed solutions for different junction geometries and boundary conditions are also given. Our preliminary conclusions are presented in Section 5 together with our future research plans.

2. Derivation of the Josephson junction PDE model. A Josephson junction is a weak link between two super-conductors allowing for the coupling of electron pairs. Josephson [6] showed that the electrodynamics of such a device are described not by current and voltage but by their integrals, charge and phase which he showed to be proportional to the phase of the macroscopic wave functions of the electron pairs in the two super-conductors. He showed that the current of pairs across the link depended on the sine of that phase difference. These two relations allow the device to act as a frequency-voltage convertor leading to applications like high frequency oscillators, fast switches or the definition of a voltage standard ([14],[7], [2]). Another effect is

* Laboratoire de Mathématiques, Institut de Sciences Appliquees, BP8, 76131 Mont-Saint-Aignan Cedex, France. (*caputo@lmi.insa-rouen.fr*)

† Physics Department, University of Crete, Heraklion, Greece. (*flytzani@minos.cc.uch.gr*)

‡ Purdue University, Computer Science Department,West Lafayette, IN 47907, USA. (*mav@cs.purdue.edu*) Work supported in part by National Science Foundation grant CCR 92-02536.

FIG. 1. *A window Josephson junction.*

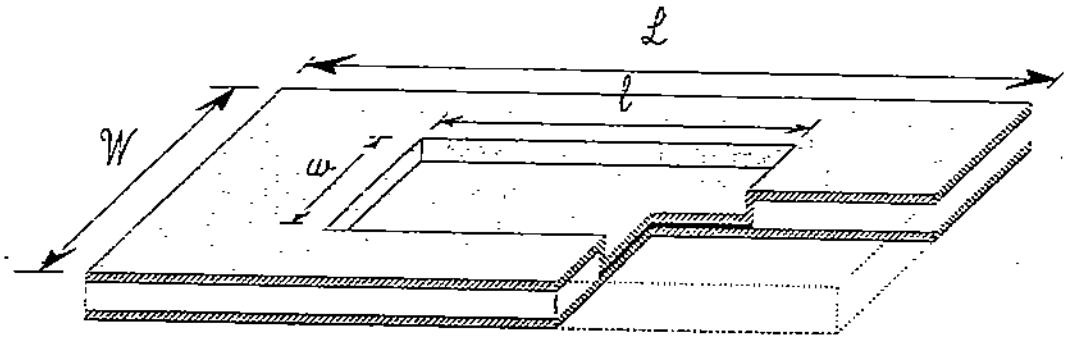

the existence of a current of pairs in the absence of voltage. This current can be modulated into an interference pattern by an external magnetic field making these devices very sensitive magneto-meters [2]. For an isolated junction these effects remain small energetically and an idea to increase the energy output is to have them drive an electro-magnetic cavity. In practice this is done by making the top and bottom super-conducting layers much larger than the junction area. This design leads to very well controlled specifications and the junctions do not deteriorate with time. A view of such a device is presented in Figure 2. In this work we model such type of junction and find the static (zero voltage) solutions. The properties of these solutions can be verified experimentally and from a different point of view these static solutions provide adapted initial conditions for the time-dependent problem.

The governing equations of such a device are Maxwell's equations together with the Josephson equations mentioned above. Design issues and the fact that the thickness of the weak link (oxide layer) is very small, force the fields to be in a plane. One can then model each super-conducting layer by an array of inductances and their coupling by a non-linear element given by the Josephson equations in parallel with a resistor representing the current of normal electrons and a capacity [7]. Writing the equations for the phase difference between the top and the bottom layer, and assuming a perfect symmetry for the parameters we get the model presented in Figure 2. The Kirchoff laws for this array can be condensed into the following discrete evolution equation for the phase Φ_i (integral of the voltage) at each node i of the array:

$$(1) \qquad -\sum_{\text{nearest neighbors j}} \frac{\Phi_i - \Phi_j}{L_{ij}} + C\ddot{\Phi}_i + \frac{\Phi_0}{L_i\lambda^2}\sin(\frac{\Phi_i}{\Phi_0}) = I_i^{\text{ext}}.$$

This equation expresses the fact that the algebraic sum of all currents is zero at a given node. The first term corresponds to the current in the inductances (surface current),

FIG. 2. *The equivalent circuit model.*

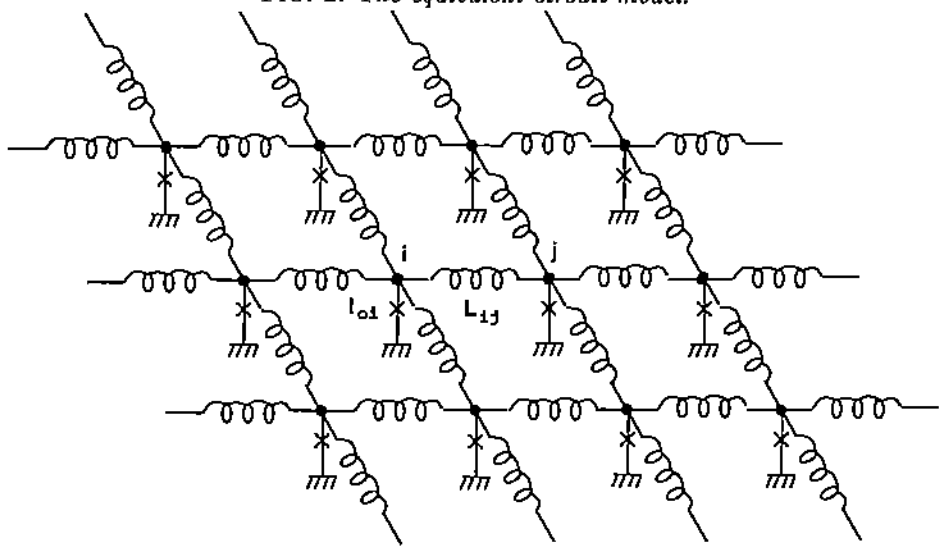

the second is the current in the capacitance and the third is the current of pairs which exists only in the junction region. The last term I_i^{ext} is an external current applied symmetrically to the boundary of the array and it can also describe the effect of an external magnetic field if applied antisymetrically [9]. The physical parameters are, L_{ij} the inductance in branch ij , C the capacitance at node i, λ the Josephson length, L_i the inductance in each branch, Φ_0 the quantum of flux. The time independent problem gives rise to a discrete semi-linear elliptic equation which reduces in the continuum limit to :

$$(2)\quad \nabla\left(\frac{1}{\mathrm{L(x,y)}}\nabla u\right) - \epsilon(x,y)\frac{1}{\lambda^2 \mathrm{L(x,y)}}\sin(u) = 0 \ \text{ in } \ \Omega, \qquad \frac{\partial u}{\partial n} = f(x,y) \ \text{ on } \ \partial\Omega,$$

where $\epsilon(x,y)$ is the indicator function of Ω_J. i.e.

$$\epsilon(x,y) = \begin{cases} 1 & \text{if}(x,y) \in \Omega_j \\ 0 & \text{otherwise} \end{cases}$$

and where $\frac{\partial}{\partial n}$ denotes the outward normal derivative. When considering a device such as the one in Figure 1 with a total area Ω and a junction area Ω_J the function L assumes a constant value in Ω and another constant value in Ω/Ω_J. Then equation (2) reduces to the boundary value problem which can be expressed formally as

$$(3)\quad \nabla([\epsilon + k(1-\epsilon)]\nabla u) - \epsilon(x,y)\frac{1}{\lambda^2}\sin(u) = 0 \ \text{ in } \ \Omega, \qquad \frac{\partial u}{\partial n} = f(x,y) \ \text{ on } \ \partial\Omega,$$

where $k = \frac{L_{\text{in}}}{L_{out}}$ and where L_{in} and L_{out} are the inductances inside and outside the junction Ω_J respectively. This PDE problem is equivalent to the composite system:

$$(4)\qquad \Delta u_{in} = \frac{\sin(u_{in})}{\lambda^2} \ \text{ in } \ \Omega_J$$

$$\Delta u_{out} = 0 \text{ in } \Omega/\Omega_J \tag{5}$$

coupled with the following interface and boundary conditions

$$\frac{\partial u_{in}}{\partial n} = k\frac{\partial u_{out}}{\partial n} \text{ on } \partial\Omega_J, \quad \frac{\partial u_{out}}{\partial n} = f \text{ on } \partial\Omega. \tag{6}$$

To show this equivalence one derives the jump condition on the normal derivative from (3). We integrate the operator (3) on a small surface element of size a in the x direction and b in the y direction overlapping the top interface. Then we apply Green's theorem to get that

$$\int_{\partial S}(\epsilon + k(1-\epsilon))\nabla u \, \mathbf{n} ds = \oint_S \frac{\epsilon \sin(u)}{\lambda^2} ds. \tag{7}$$

Placing the middle of the square on the origin we obtain that

$$\int_0^{\frac{b}{2}}(1-k)\left(\frac{\partial u}{\partial x}(\frac{a}{2},y) + \frac{\partial u}{\partial x}(\frac{-a}{2},y)\right)dy + + \int_{-\frac{a}{2}}^{\frac{a}{2}} + \left(\frac{\partial u}{\partial y}(x,-\frac{b}{2}) + k\frac{\partial u}{\partial y}(x,\frac{b}{2})\right)dx \tag{8}$$

$$-\frac{1}{\lambda}\int_{-\frac{a}{2}}^{\frac{a}{2}}\int_{-\frac{b}{2}}^{0}\sin(u)dxdy = 0. \tag{9}$$

Taking the limit $b \to 0$ we get that $\forall a \in R$

$$\int_{-\frac{a}{2}}^{\frac{a}{2}}\left(\frac{\partial u}{\partial y}(x,0^-) + k\frac{\partial u}{\partial y}(x,0^+)\right)dx = 0 \tag{10}$$

which implies the above mentioned jump condition.

The form (3) cannot be implemented in practice because of the discontinuity in ϵ, one has to use the composite system (5) except in the case $k = 1$. In that case (3) takes the simple form

$$\Delta u = \epsilon\frac{sin(u)}{\lambda^2} \text{ in } \Omega, \quad \frac{\partial u}{\partial n} = f(x,y) \text{ on } \partial\Omega. \tag{11}$$

This PDE can be solved numerically as is except for the fact that one has to make sure that no discretization points are on the interface where the operator is not defined.

If we integrate the operator (11) over Ω and apply Green's theorem we get

$$\int_\Omega sin(u)dxdy = \oint_{\partial\Omega} f(x,y)ds. \tag{12}$$

This quantity is the total current of pairs across the junction, it is also the total current because there is zero voltage so that there is no electronic current.

Another way of studying the problem is to use a variational approach. The energy of the system given in Figure 2 in the absence of external currents is

$$E_{\text{dis}} = \sum_{i,j}\frac{1}{2L_{ij}}(\Phi_i - \Phi_j)^2 + \sum_i \frac{\Phi_0^2}{L_i\lambda_j^2}\left(1 - \cos(\frac{\Phi_i}{\Phi_0})\right). \tag{13}$$

The first sum is over nearest neighbors and corresponds to the energy stored in the inductances. These are surface currents on each of the super-conductors. The second term corresponds to the current of pairs and exists only in the junction. When scaling all the parameters and going to the continuum limit for a device of total surface Ω and area of the junction Ω_J one gets:

$$(14) \qquad E = \int_\Omega \frac{1}{2}(\nabla u)^2[\epsilon + k(1-\epsilon)] + \frac{\epsilon}{\lambda_j^2}(1-\cos(u))dxdy \qquad \frac{\partial u}{\partial n} = 0 \ \text{ on} \partial\Omega.$$

The solution of (11) with a non zero boundary condition does not correspond in general to a minimum (or even an extremum) of the functional (14). When writing that the variation of (14) is zero one obtains by integrating by parts:

$$(15) \int_\Omega [-\frac{\partial}{\partial x}(u_x) - \frac{\partial}{\partial y}(u_y) + \epsilon\frac{\sin(u)}{\lambda^2}]\ \delta u dxdy = \oint_{\partial\Omega} \nabla u \ \mathrm{n}\ \delta u ds = \oint_{\partial\Omega} f(x,y)\ \delta u\ ds.$$

When $f = 0$ one recovers (11) from the second lemma of calculus of variations [13]. When f is different from zero the integral is not zero except if the solution and the domain present some symmetries. This is the case when Ω is a rectangle, when Ω_J is symmetric and centered and when f is distributed symmetrically on the top and bottom boundaries of Ω. Then the solution of (11) is obviously symmetric so that δu is symmetric and the integral is zero. This corresponds to applying an external magnetic field to the junction. Assuming the same geometry together with an antisymmetric solution in the x direction and an antisymmetric distribution for f on the left and right boundaries leads again to a minimum. This corresponds to a non zero total current crossing the junction.

In the next section we will derive iterative methods for solving the PDE problem (11) numerically. All these iterative methods require an initial guess $u^{(0)}$ while some of them will diverge if this initial guess is far away from the true solution.

An initial condition is chosen so as to conform to the well known [2] one dimensional solution of the sine-Gordon equation $\frac{\partial^2 u}{\partial x^2} = \frac{\sin(u)}{\lambda^2}$ in the case of infinite boundaries

$$(16) \qquad u^{(0)}(x,y) = 4\arctan(e^{\pm\frac{x}{\lambda}})$$

A better way of choosing the initial guess would be to use the approximate electrostatic model given in [3] which consists of approximating the solution by (16) with a width α instead of λ in Ω_J and take an appropriate electrostatic solution in Ω/Ω_J.

It should be pointed out that the above described initial guesses may lead us to a diverging iteration sequence when the external current (I_i^{ext} in (1)) we apply on the boundary $\partial\Omega$ is large. In this case we first solve the problem with relatively small external current and then we fit the computed solution as initial guess to the same problem with increased current.

3. Numerical Algorithms and Implementations. In this section we formulate an efficient and stable numerical method for solving the semi-linear Elliptic Partial

Differential Equation (PDE) problem (11). One can linearize the PDE equation by means of the following fixed point iteration scheme.

$$(17)\quad \lambda^2\Delta u^{(i)} - \epsilon(x,y)r(x,y)u^{(i)} = \epsilon(x,y)\left(\sin(u^{(i-1)}) - r(x,y)u^{(i-1)}\right),\ i = 1,2,\ldots$$

where $r(x,y)$ is a relaxation function to accelerate the convergence and it can be any positive function.

Although the convergence analysis of this iteration method will be presented in detail elsewhere we should state here that, in the case where $r(x,y)$ is a positive constant c it is easy to see the convergence of the resulting iteration scheme.

THEOREM 3.1. *Denote the operator L such that $Lu \equiv \lambda^2\Delta u - c\epsilon u$ and assume that $||u^{(i)} - u|| \leq d||L\left(u^{(i)} - u\right)||$. The iteration method defined by (17) starting from an initial guess $u^{(0)}$ such that $||\sin(u^{(0)}) - \sin(u)|| \leq ||u^{(0)} - u||$, converges to the solution of the PDE problem (11) if c is selected such that $|d(1+c)| < 1$.*

Proof: We first see that

$$(18)\qquad L\left(u^{(i)} - u\right) = \epsilon\left\{\left[\sin(u^{(i-1)}) - \sin(u)\right] + c\left[u^{(i-1)} - u\right]\right\}.$$

Then we have that

$$(19)\quad ||u^{(i)} - u|| \leq d||L\left(u^{(i)} - u\right)|| \leq d\left\{||\sin(u^{(i-1)}) - \sin(u)|| + c||u^{(i-1)} - u||\right\}.$$

from which we can obtain that

$$(20)\qquad ||u^{(i)} - u|| \leq [d(1+c)]^i||u^{(0)} - u||.\square$$

For the implementation the optimum value for the parameter c depends on λ and the discretization parameter n.

For $r(x,y) = \cos(u(x,y))$ the iteration scheme (17) reduces to the well known Newton's iterative method [8]. The analysis of this rapidly converging (second order) scheme following the technique found in [1] is under way and it will be presented elsewhere.

For any $r(x,y) \neq 0$ we have the following scenario. The first solution phase of the numerical process we are proposing is to replace the linear continuous PDE problem, which is involved within each iteration step in (17), with a discrete one which approximates it. Through this phase, called discretization, we obtain a system of linear algebraic equations. The unknown vector vector of the produced system determines a discrete approximation of the solution of the continuous problem.

More specifically, first we discretize the PDE domain by placing a non-uniform rectangular grid (or a set of elements) over it. It is worth to point out that for the accuracy and the stability of our scheme this domain discretization may need to be fine enough along the junction where the solution is expected to vary rapidly. This domain discretization is then used by a numerical method (finite difference, finite element or collocation) to replace the linear PDE equation and the boundary conditions by a linear system of algebraic equations $A\mathbf{x} = \mathbf{b}$. These equations may need to be modified to satisfy jump conditions of the form $\frac{\partial u}{\partial n} = k\frac{\partial u}{\partial n}$ that correspond to the continuity of the normal component of the surface current across the junction.

The second phase involves only linear algebra computations. First we factorize the matrix $A = LU$ using Gauss elimination. The fixed point iterations start then. Within each iteration we first use the current approximation of the vector $\mathbf{x}$ to compute the updated value of the right hand side vector $\mathbf{b}$. Then the linear system $LU\mathbf{x} = \mathbf{b}$ is solved using backward/forward substitution.

We start the iterations using an initial guess $u^{(0)}$ of the solution u obtained using one of the approaches described in the previous section. We terminate the iteration procedure when the max-norm of the difference of two successive approximations of the solution vector $\mathbf{x}$ is less than a given tolerance.

We have implement the proposed method in the ELLPACK framework [10], [5]. The ELLPACK program that implements the above presented solution scenario is given below after discarding few unimportant statements and routine arguments.

```
EQUATION.          uxx + uyy - eps(x,y)*cos(u(x,y))*u = &
                      eps(x,y)*( sin(u(x,y))-u(x,y)*cos(u(x,y)) )
BOUNDARY.          ux = f(x,y) on y = 0. $ on y = 1.
                   uy = f(x,y) on x = 0. $ on x = 2.
GRID.              nxpt x points $ nypt y points
DISCRETIZATION. 5 point star
TRIPLE.            set( u = u_init )
FORTRAN.
                   call factor( )
                   do 100 niter = 1, maxiters
                      call back_solve( )
                      call update_rhs( )
                      call check_convergence( )
100                continue
200                call print_summary( )
VISUALIZATION.     xplot3d(u) $ xplot3d(energy)
SUBROUTINES.
                   ⋮
```

It is worth noticing that the floating point computational complexity of this implementation is bounded by $\frac{n^3}{3} + k\frac{n^2}{2}$ where $n = nxpt \times nypt$ and k is the number of iterations required for convergence.

4. Numerical Experiments. In this section we present the results of some numerical experiments that verify the convergence properties of the iterative solution methods of Section 3 and exhibit the modelling power of our scheme. All experiments were performed using single precision on a SUN 4.

4.1. Convergence and efficiency of the method. To confirm the efficiency and the stability of the method we described we present in this section some preliminary numerical results.

TABLE 1
The value of $||u^{(i)} - u^{(i-1)}||_{max}$ *for different grid sizes.*

	GRID SIZE				
iteration	20×20	40×40	60×60	80×80	100×100
1	6.265	6.266	6.266	6.266	6.266
2	2.154E-2	2.740E-2	2.783E-2	2.844E-2	2.842E-2
3	8.630E-5	1.068E-4	1.225E-4	1.134E-4	1.306E-4
4	2.384E-6	4.291E-6	8.583E-6	9.060E-6	1.001E-5
5	1.430E-6	3.338E-6	7.096E-6	7.629E-6	8.049E-6

FIG. 3. *Total elapsed time in seconds required for* $||u^{(i)} - u^{(i-1)}||_{max} < 10^{-5}$.

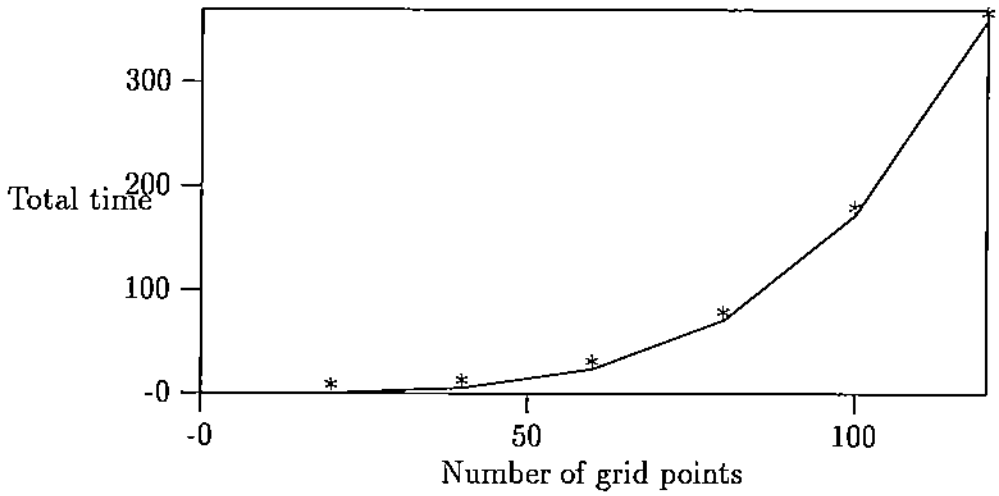

We have considered the PDE problem (11) with $\Omega = [0,2] \times [0,1]$, $\Omega_J = [.5,1.5] \times [.3,.7]$, $\lambda = .05$ and $f(x,y) \equiv 0$. The ELLPACK program whose main segment was given in the previous section was used. Thus we used a uniform domain discretization grid with *nxpt*, *nypt* grid points in x and y directions respectively and $r(x,y) = cos(u(x,y))$.

Table 1 presents the convergence behavior of the method. As it can be easily seen the iteration scheme converges very rapidly, while the increase of the number of grid points have very little affect on the rate of convergence. It is worth pointing out that the discrete (on the discretization grid) norm of the computed residual upon convergence agrees with the theoretically expected truncation error of the five point star discretization method.

The computational complexity of the method given in the previous section can be numerically verified from Figure 3 where we plot the total elapse CPU time in seconds versus the number of grid points $n = nxpt = nypt$.

4.2. Computed solutions. Our first objective is to study the influence of the shape of Ω_J on the solution, for homogeneous boundary conditions. In this case the

TABLE 2

The computed values for various energy quantities for junctions of different geometries but the same area.

Energies	Rectangular	Ellipse	Oval
Total Magnetic	32.26	32.50	35.78
Josephson	5.87	12.18	20.71
Magnetic inside	4.79	8.62	15.96
Magnetic outside	27.47	23.88	19.82
Total	38.13	44.68	56.49

solution minimizes the energy E given in (14) with $k = 1$. As we can see E consists of two terms. The first term $em = \int_\Omega \frac{(\nabla u)^2}{2} dxdy$ is minimum when the solution is flat while the second term $ej = \int_{\Omega_J} \frac{\sin(u)}{\lambda^2} dxdy$ when the solution varies abruptly for 0 to 2π. The solution results from the competition between these two terms which depends on the shape of Ω_J.

We have considered three different cases for the junction Ω_J namely, a rectangle $[.5, 1.5]$, an ellipse with half axis $a = .6366$ and $b = .1$ and a Cassini oval [11] which realizes a bow-tie type geometry with half width varying in [.1,.16] and half lenght .408. For all three junctions we have fixed the half width to .1 and kept the area equal to .2. The reason for the above choices is that the energies strongly depend on the ratio of the widths of Ω and Ω_J [3] and we kept the amount of material for Ω_J constant.

In Table 2 the following energies are given

- Total magnetic energy em,
- Josephson energy ej,
- Magnetic energy inside $emj = \int_{\Omega_J} \frac{(\nabla u)^2}{2} dxdy$,
- Magnetic energy outside $emout = \int_{\Omega/\Omega_J} \frac{(\nabla u)^2}{2} dxdy$ and
- Total energy $et = em + ej$.

In the case of a rectangular geometry it is possible to estimate the average features of the solution using a simple electrostatic analog [3] and assuming that the solution has the form given in (16) in Ω_J with half length α. Then we have that

$$em = emj + emout \approx \frac{4w}{\alpha} + 4\pi \log\left(\frac{\ell}{2\alpha}\right), \tag{21}$$

where w is the width of Ω_J and ℓ is its length. The value of α which minimizes the total energy $et = em + ej$ is $\alpha = \frac{\pi\lambda^2}{w}(1 + \sqrt{1 + \frac{4w^2}{\pi^2\lambda^2}})$ where w is the width of Ω_J. We see the good agreement of the energies of the computed solution for the first column of table 2 with this simple model. Another observation that can be made is that for a given area and middle width the oval is the shape that carries the most energy.

Next we examine the general features of the computed solutions. In Figure 4 we give the 3-dimensional and contour plots of the solution which ranges in $[0, 2\pi]$ together with the magnetic energy density $med = \frac{(\nabla u)^2}{2}$ and the current of pairs $cur = \epsilon \frac{\sin u}{\lambda^2}$. In Figure 5 we present the first and second partial derivatives of the solution in the x

and y directions. The second derivatives are clearly discontinuous along the respective boundaries of Ω_J while the first ones seem to be continues but rapidly varying. Figure 6 presents the contour plots for the solution for the ellipse and the oval together with the super-current. We should point out that the latter function is anti-symmetric with respect to $x = 1$, resulting in a null total current crossing the junction as can be expected from the fact that the boundary conditions are homogeneous.

Finally in Figures 8 and 7 we consider the rectangular case and study the effect of non-homogeneous boundary conditions. Specifically we impose anti-symmetric boundary conditions on $y = 0$ and $y = 1$ together with symmetric boundary conditions on $x = 0$ and $x = 2$. Physically this corresponds to applying an external magnetic field in the y direction and assuming a total super-current collected from $y = 0$ on the top super-conductor and $y = 1$ on the bottom super-conductor. In Figure 7 we have assumed a zero magnetic field and super-current of amplitude 1. Figure 8 corresponds to the same configuration with a non zero external magnetic field applied along the left and right boundaries of Ω. This corresponds to a symmetric boundary condition on the left and right boundaries.

5. Conclusions and future work. In a future work we will address the important question of the smoothness of the solution, in particular show that it is C^1 when $k = 1$ and C^0 when $k \neq 1$. Concerning the numerical algorithm it should be pointed out that several modifications can be easily derived by using:

- Domain decomposition techniques that will separate the original PDE problem (11) into a linear and a non-linear one ([4]). This will be particularly suited to the case $k \neq 1$.
- Different than Gauss Elimination based linear solvers for the algebraic equations (e.g. Preconditioning Conjugate Gradient, GMRES).
- Different than 5 point star discretization methods.
- Different than $sin(u)$ relaxation factor in (17).

We will report on these modifications and present the convergence analysis of the proposed methods elsewhere.

Future numerical experiments will address the issue of the optimal shape for Ω_J in the case of homogeneous boundary conditions. When λ gets larger than the width of Ω_J the solution tends to flatten out along the junction [3]. This effect seems to depend strongly on the shape of Ω_J, for a given λ the ellipse will yield a flatter solution than the bow-tie geometry. Another situation that can be studied very easily by changing ϵ is when there are several subdomains $\Omega_J^1, \Omega_J^2 ...$ in Ω.

In the case of non-homogeneous boundary conditions it has been shown in one dimension [9] and confirmed experimentally [12] that for a given magnetic field there is a maximum total current crossing the junction. This maximum current displays an interference like pattern when the external magnetic field is varied. We will calculate this for a typical window junction adapting the initial guess as discussed in section 3 to ensure convergence. This will be done for different electrode configurations.

FIG. 4. *The 3-dimensional and the contour plots of the computed solutions u, the magnetic energy density and the super-current for a rectangular junction $\Omega_J = [.5, 1.5] \times [.4, .6]$, with $\lambda = .05$ and homogeneous boundary conditions*

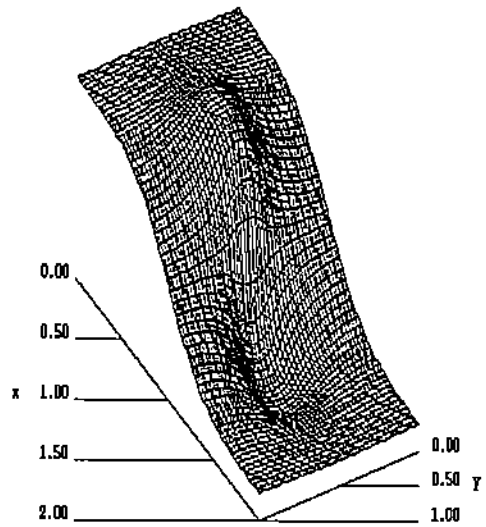

u (ranging in [0,2π]).

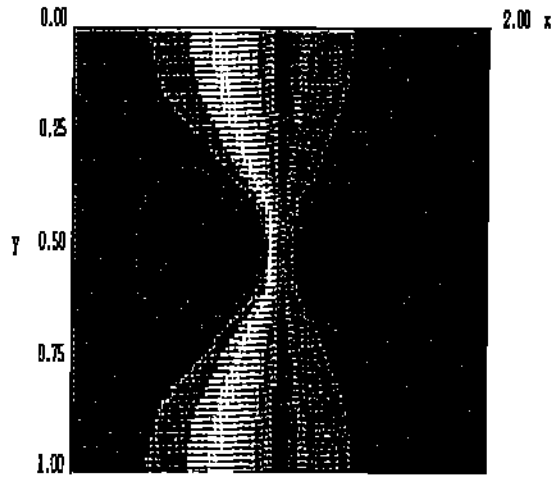

contour plot of u.

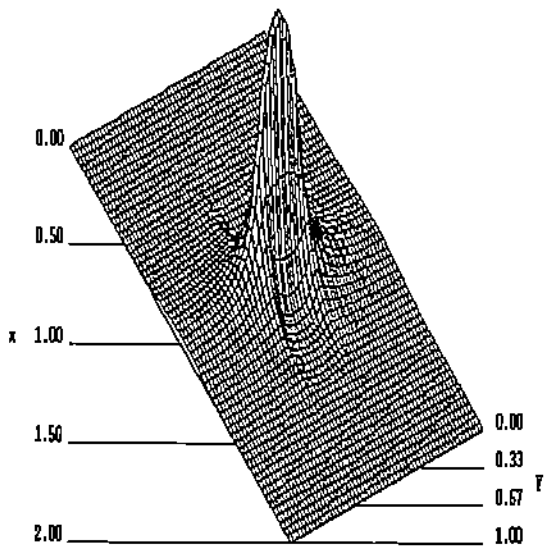

Energy density.

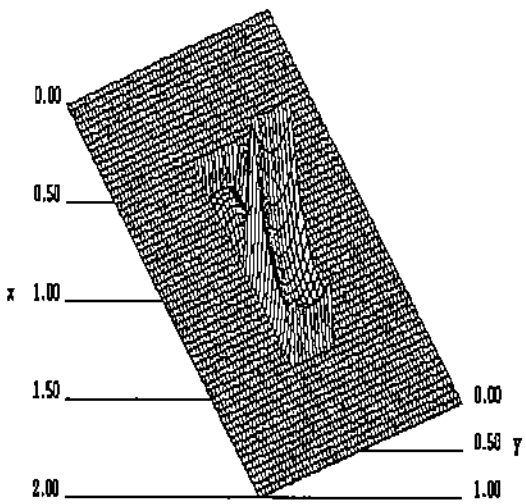

Super-current.

FIG. 5. *The first and second derivatives of the computed solution u for the problem considered in Figure 4.*

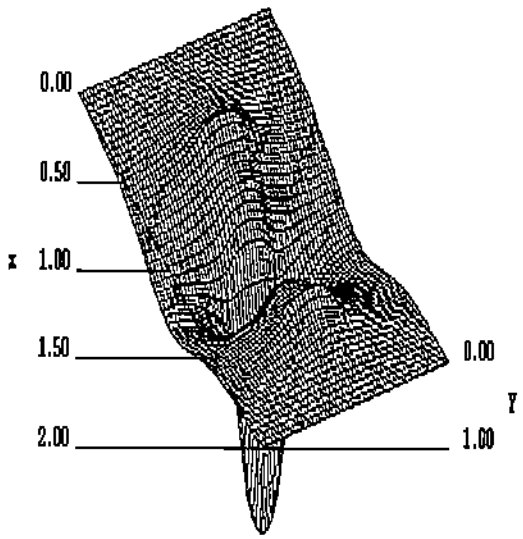

$\frac{\partial u}{\partial x}$(ranging in [-37,1.33])

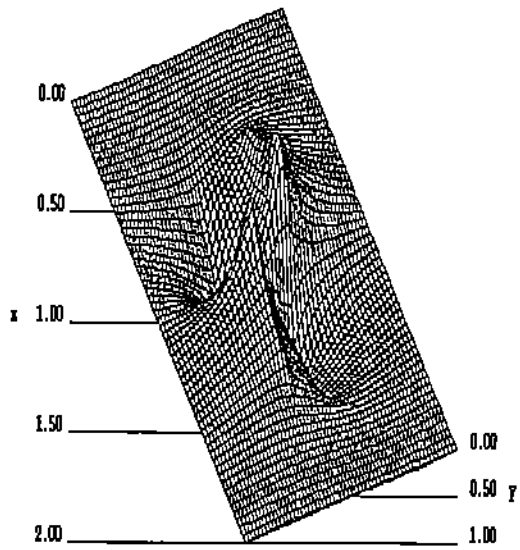

$\frac{\partial u}{\partial y}$(ranging in [-11,11])

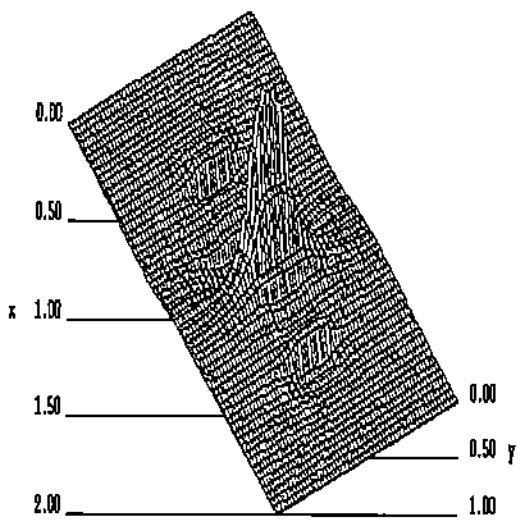

$\frac{\partial^2 u}{\partial x^2}$ (ranging in [-390,390])

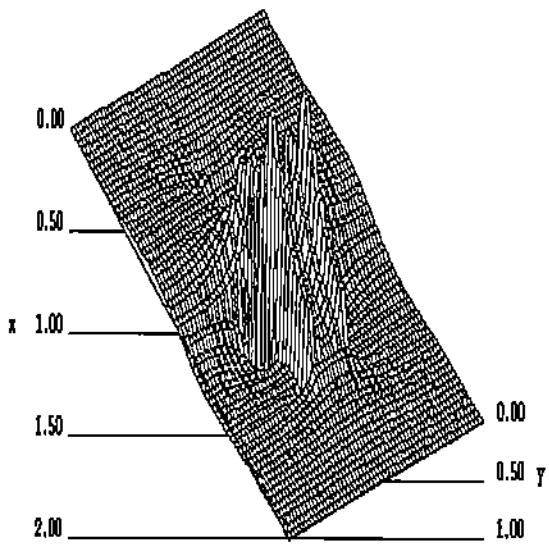

$\frac{\partial^2 u}{\partial y^2}$ (ranging in [-171,171])

FIG. 6. *Contour plots and 3-dimensional plots for the computed solution and the super-current respectively with the junctions being ellipse and oval.*

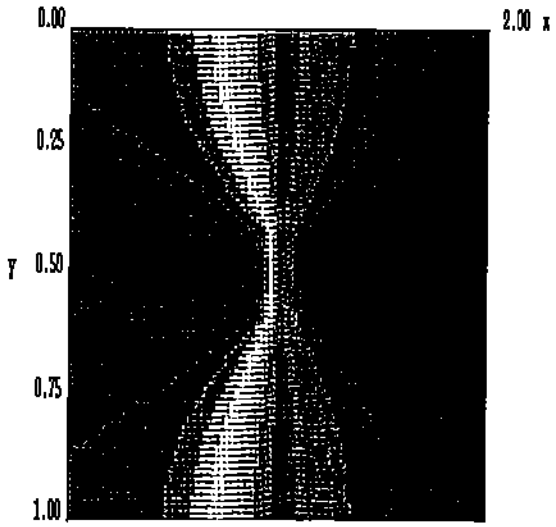

u for the elliptic junction.

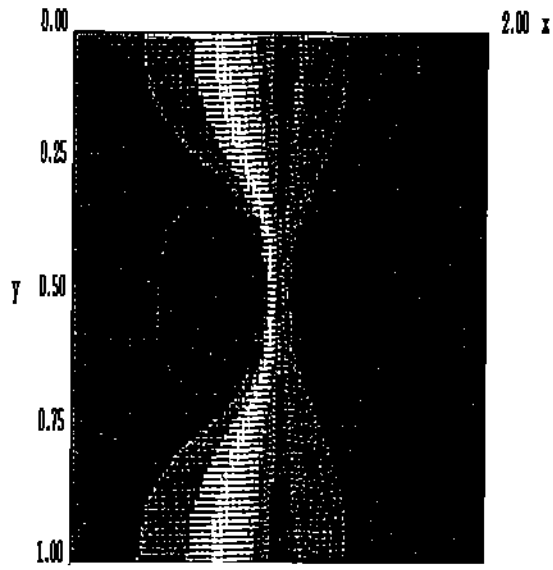

u for the oval junction.

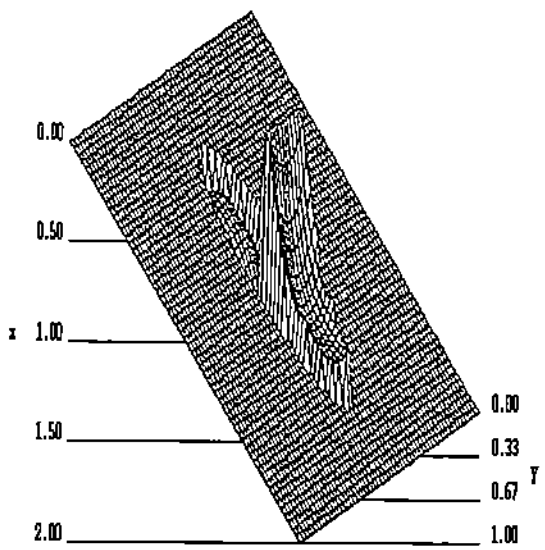

Super-current for the elliptic junction.

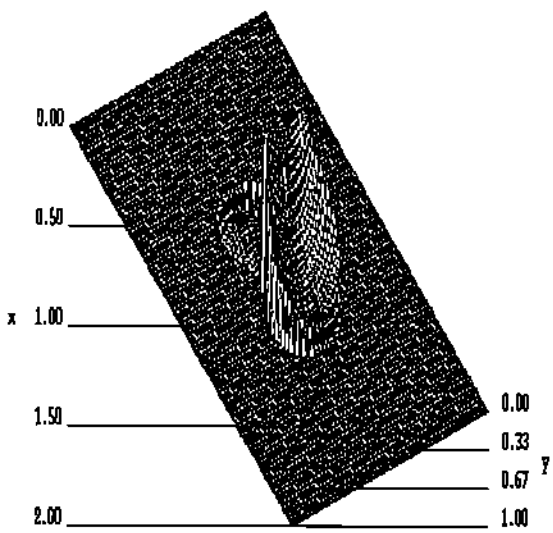

Super-current for the oval junction.

FIG. 7. *3-dimensional and contour plots of the computed solution u and the super-current for the rectangular junction assuming a non zero total current without external magnetic field.*

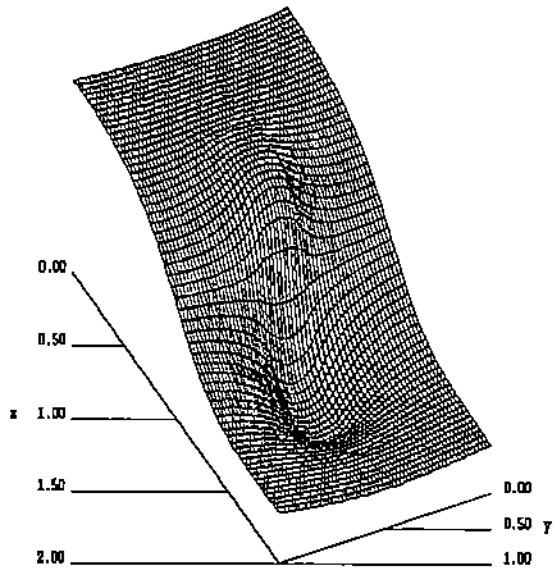

u

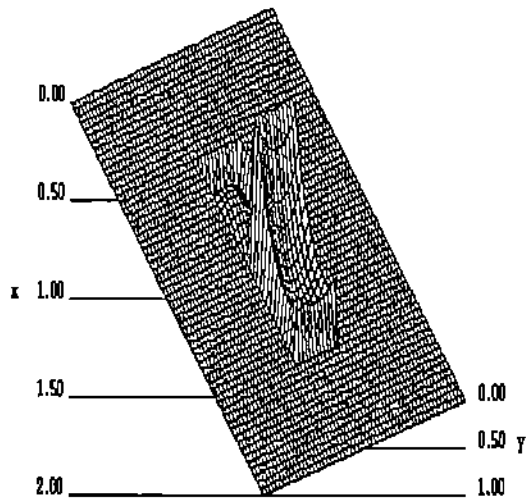

Super-current.

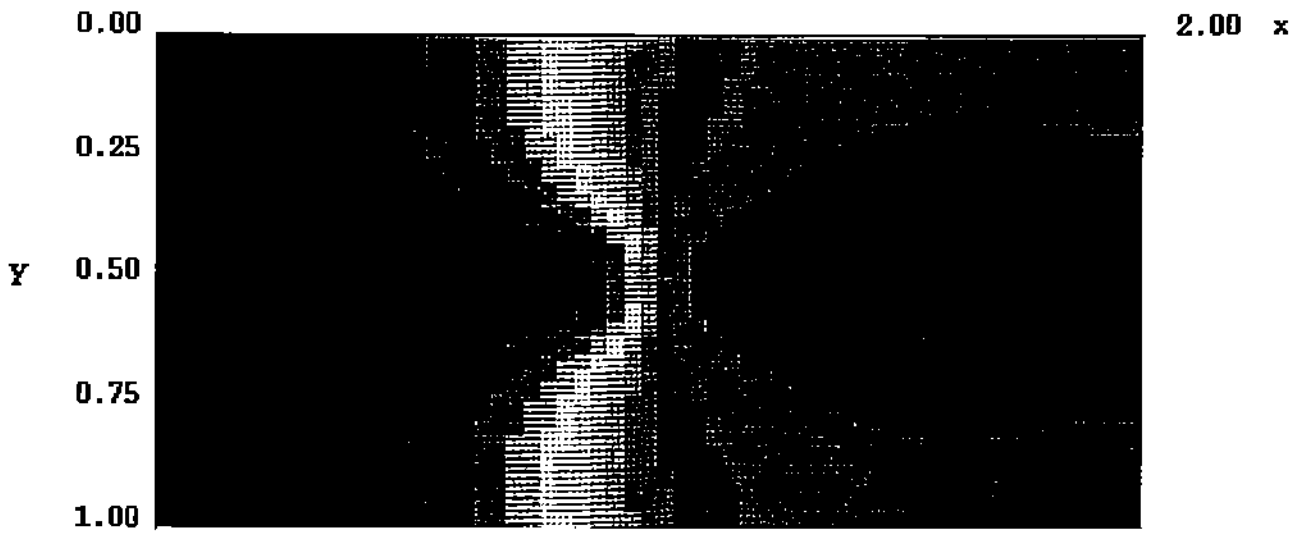

Contour plot of u.

FIG. 8. *3-dimensional and contour plots of the computed solution u and the super-current for the rectangular assuming a non zero total current and an external magnetic field.*

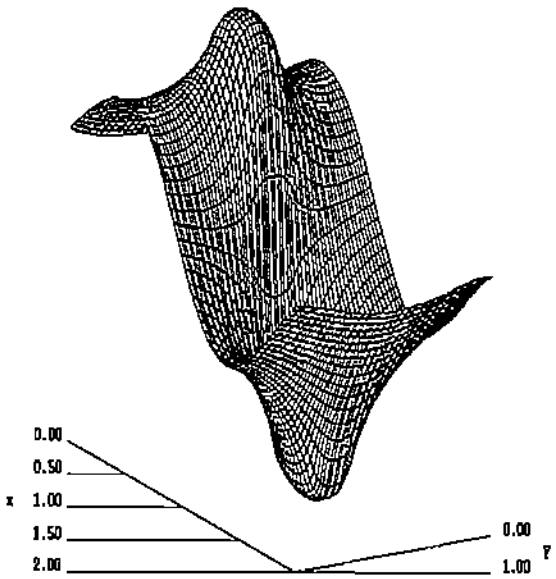

u.

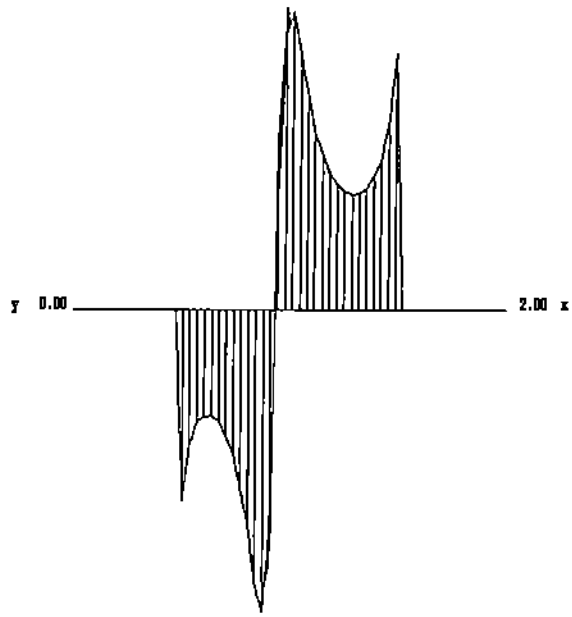

Super-current.

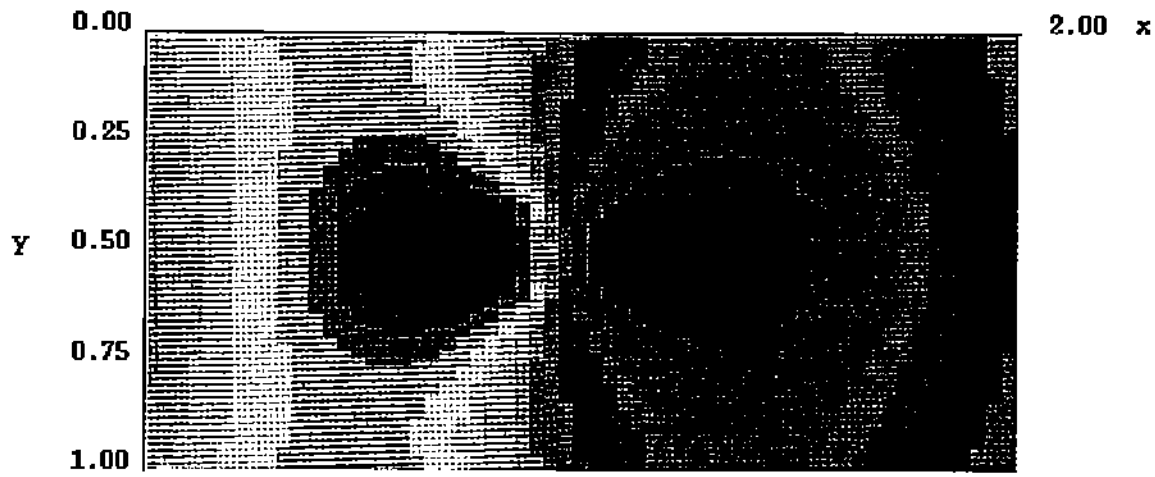

Contour plot of *u*.

REFERENCES

[1] C. Ablow and C. Perry, *Iterative solution of the Dirichlet problem for $\delta u = u^2$*, J. Soc. Indust. Appl. Math., 7 (1959), pp. 459–467.

[2] A. Barone and G. Paterno, *Physics and Applications of the Josephson effect*, John Wiley, New York, 1982.

[3] J. G. Caputo, N. Flytzanis, and M. Devoret, *Static solutions of a two-dimensional josephson window junction*, in Future directions of non linear dynamics in physical and biological systems, 1992.

[4] C. Christara, A. Hadjidimos, E. Houstis, J. Rice, and E. Vavalis, *Geometry decomposition based methods for solving elliptic PDEs*, in Comp. Methods in Flow Analysis, vol. 2, Univ. of Okayama, Japan, 1988, pp. 175–182.

[5] E. Houstis, J. Rice, N. Chrisochoidis, H. Karathanasis, P. Papachiou, E. Vavalis, and K. Wang, *(//) ELLPACK: A numerical simulation programming environment for parallel MIMD machines*, in Supercomputing 90, ACM Press, pages 96–107, 1990.

[6] B. Josephson, *Possible new effects in superconductive tunelling*, Phys. Lett., 1 (1962), pp. 251–253.

[7] K. Likharev, *Dynamics of Josephson junctions and circuits*, Gordon and Breach, New York, 1986.

[8] J. Ortega and W. Rheinboldt, *Iterative Solution of nonlinear equations in several variables*, Academic Press, New York, 1970.

[9] C. Owen and D. Scalapino, *Vortex structure and critical currents in josephson junctions*, Phys. Rev., 164 (1967), pp. 538–544.

[10] J. Rice and R. Boisvert, *Solving Elliptic Problems Using ELLPACK*, Springer-Verlag, New York, 1985.

[11] G. Salmon, *Higher plane curves*, G. E. Stechert, 1934.

[12] K. Schwidtal, *Type I and type II superconductivity in wide josephson junctions*, Phys. Rev. B, 2 (1970), pp. 2526–2532.

[13] D. Simth, *Variational methods in optimisation*, Prentice-Hall, Inc., New Jersey, 1974.

[14] T. Van Duzer and C. Turner, *Priciples of superconducting devices and circuits*, Edward Arnold, 1987.